Chem Biol Drug Des 2006; **67:** 346–354

doi: 10.1111/j.1747-0285.2006.00387.x

Research Article

Insight into the Binding Mode for Cyclopentapeptide Antagonists of the CXCR4 Receptor

Jon Våbenø, Gregory V. Nikiforovich and Garland R. Marshall*

Department of Biochemistry and Molecular Biophysics, Center for Computational Biology, Washington University School of Medicine, 700 South Euclid Avenue, St Louis, MO 63110, USA
**Corresponding author: Garland R. Marshall, garland@pcg.wustl.edu*

The finding that the chemokine receptor CXCR4 is involved in T-cell HIV entry has encouraged the development of antiretroviral drugs targeting this receptor. Additional evidence that CXCR4 plays a crucial role in both angiogenesis and metastasis provides further motivation for the development of a CXCR4 inhibitor for therapeutic applications in oncology. To facilitate the design of such ligands, we have investigated the possible binding modes for cyclopentapeptide CXCR4 antagonists by docking 11 high/medium affinity cyclopentapeptides to a developed three-dimensional model of the CXCR4 G-protein-coupled receptor's transmembrane region. These ligands, expected to bind in the same mode to the receptor, were docked in the previously deduced receptor-bound conformation [Våbenø *et al.*, in press; doi 10.1002/bip.20508]. Ligand–receptor complexes were generated using an automated docking procedure that allowed ligand flexibility. By comparing the resulting ligand poses, only two binding modes common for all 11 compounds were identified. Inspection of these two ligand–receptor complexes identified several CXCR4 contact residues shown by mutation to be interaction sites for ligands and important for HIV gp120 binding. Thus, the results provide further insight into the mechanism by which these cyclopentapeptides block HIV entry as well as a basis for rational design of CXCR4 mutants to map potential contacts with small peptide ligands.

Key words: angiogenesis, binding mode, CXCL12, CXCR4 antagonists, cyclopentapeptides, docking, homology modeling, human immunodeficiency virus, metastasis, receptor-bound conformation, stromal cell-derived factor-1α

Received 1 May 2006, revised and accepted for publication 1 May 2006

In addition to its physiological role as the sole receptor for the chemokine stromal cell-derived factor-1α (SDF-1α; officially CXCL12) (1,2), the G-protein-coupled receptor (GPCR) CXCR4 is the coreceptor for the entry of T-tropic human immunodeficiency virus (HIV) strains into $CD4^+$ T cells (3,4). As HIV infection of T cells is associated with a rapid deterioration of the immune system leading to progression towards the disease stages associated with acquired immunodeficiency syndrome (AIDS) (5–11), the CXCR4 receptor has emerged as a potential target for HIV/AIDS therapy. Accordingly, a large number of CXCR4 antagonists have been described, including mono-/bicyclams [AMD series, AnorMED (Langley, BC, Canada); for a review, see Ref. (12)], Arg-based peptidomimetics [KRH series, Kureha Chemical Industries (Tokyo, Japan) (13,14)], and peptidic compounds such as ALX40-4C [Ac-(D-Arg)$_9$-NH_2 (15)] and the downsized polyphemusin derivatives developed by Fujii *et al.* [for a review, see Ref. (16)]. A common feature for all these compounds is their (poly)cationic nature, raising a possible concern for the oral bioavailability as well as for the binding specificity.

In our ongoing effort to develop a potent and orally active peptidomimetic CXCR4 inhibitor with high specificity, the highly potent cyclopentapeptide (CPP) antagonists developed by Fujii *et al.* (17–19), e.g. FC131 [c(Gly^1-D-Tyr^2-Arg^3-Arg^4-Nal^5), Nal is L-2-naphthylalanine; Figure 1], represent a natural starting point. We have recently reported a minimalistic three-dimensional (3D) pharmacophore model for the CPPs, which suggests the spatial arrangement of the critical pharmacophoric elements required for binding to CXCR4 (20). The study was based on an exhaustive conformational search for a series of 15 CPPs, providing us with a plausible receptor-bound (bioactive) conformation, well suited for subsequent docking studies, for all the active compounds. Moreover, as CXCR4 belongs to the rhodopsin family (family A) of GPCRs, homology modeling of the CXCR4 transmembrane helix (TMH) bundle based on the X-ray structure of bovine rhodopsin (Rh) (21) was warranted. To elucidate the atomic details of ligand–receptor interactions for the CPP CXCR4 antagonists, we report the results of automated docking studies of CPP ligands to a 3D model of the CXCR4 TMH bundle. Out of the 15 CPPs included in our previous study, the 11 high/medium affinity compounds (**1**–**11**; Table 1), expected to have the same binding mode, were selected as ligands. The findings of the present study provide additional support for our recently suggested 3D pharmacophore model, as well as a basis for rational design of CXCR4 mutants to map potential contacts with small peptide ligands.

Methods

Molecular modeling of the CXCR4 TMH bundle

The general procedure for building the TMH bundle of the CXCR4 receptor was essentially the same as described previously (22,23). First, a pairwise sequence alignment of

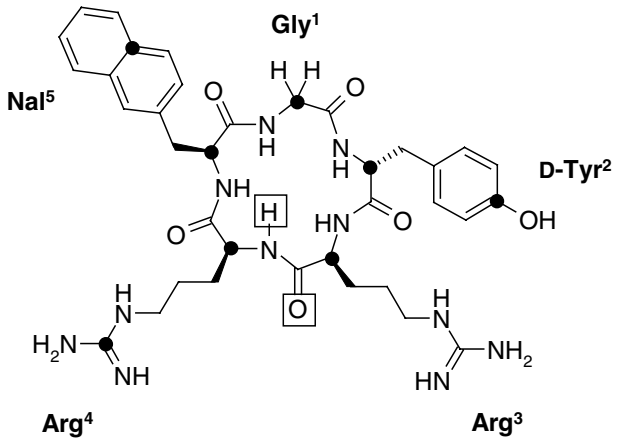

Figure 1: Structure of the cyclopentapeptide CXCR4 antagonist FC131. The 10 atoms defining the minimalistic pharmacophore model (20) are shown as eight solid circles (C atoms) and two open squares (O and H).

human CXCR4 with Rh was performed using the CLUSTAL W program (http://www.ch.embnet.org/software/ClustalW.html). With the exception of TMH4, the resulting alignment showed overlap of the CXCR4 sequence with the so-called X.50 residues of Rh, i.e. the most conserved residue in each TMH of Rh-like GPCRs [N55, D83, R135, W161, P215, P267, and P303 of Rh (24)]. Consequently, the CLUSTAL W alignment for TMH4 was shifted by one residue to achieve overlap with W161 of Rh. Assignment of the first and last residue in the TMHs of Rh was generally based on the ϕ,ψ torsions ($-20° \geq \phi,\psi \geq -100°$) of the X-ray structure [protein data bank (PDB) entry 1F88 (21); monomer A]. Minor deviations from these limitations were accepted for residues that were obviously a part of the helix, i.e. the Pro171-Leu172 fragment in TMH4 of Rh. Proline was not assigned as a TMH residue in Rh when it was located at the TMH terminus. Also, TMH1 was shortened by two residues and one residue on the extra- and intracellular sides, respectively, and the intracellular part of TMH4 was extended by one residue. This resulted in the following TMH assignment for CXCR4: TMH1: K38-T51-G64 (the first, middle, and last residues, respectively); TMH2: T73-L86-A100; TMH3: F107-S122-I138; TMH4: K149-V160-F172; TMH5: V196-L208-I221; TMH6: Q233-F248-F264; and TMH7: K282-F292-Y302 (Figure 2).

Then, the helical fragments of the CXCR4 receptor were assembled in a TMH bundle based on the following procedure: (i) determining the conformation of each individual helix by optimization of the side-chain torsions and energy minimization involving all dihedral angles, (ii) superimposing the obtained helix conformations over the X-ray structure of Rh (C^{α} atoms only) according to the alignment, and (iii) packing the seven helices into the energetically best arrangement while keeping the dihedral angles of the helical backbone fixed in the values obtained for the individual helices (step i). All energy calculations were performed with the ECEPP/2 force field, employing rigid valence geometry (25,26) and using a dielectric constant of 2.0, which is generic for the ECEPP force field. Only the *trans*-conformation of Pro amide bonds was considered, and Arg, Lys, Glu, and Asp residues were modeled as charged species. The N- and C-termini of each helix were capped with acetyl and NHMe groups, respectively.

Energy minimization for each individual TMH of CXCR4 started from the backbone conformation (ϕ, ψ, and ω dihedral angles) of the corresponding Rh helix (PDB entry 1F88A). The ϕ and ψ angles were allowed to rotate with the limitation of $-60 \pm 40°$ that, to some extent, mimics limitations on intrahelical mobility of TMHs immobilized in the membrane. For the same reason, the ω angle in Pro residues was limited to a value of $180 \pm 30°$. Side-chain torsions were optimized before and after energy minimization by an algorithm developed earlier (27). Because of an obvious distortion in the helical structure of TMH6 after this minimization procedure, the starting ψ-value for Trp^{252} was changed from $-10.6°$ to $-20.6°$ to keep its backbone angles within the limits.

Packing of the seven TMHs consisted of minimization of the sum of all intra- and interhelical interatomic energies in their multidimensional parameter space. These included the $6 \times 7 = 42$ 'global' parameters (related to the movement of the individual helices as rigid bodies, namely, translations along the co-ordinate axes *X*, *Y*, and *Z*, and rotations around these axes, T_x, T_y, and T_z) and the 'local' parameters (the dihedral angles of the side-chains for all helices). Side-chain torsions were optimized prior to each energy minimization step by an algorithm described earlier (27); see also Ref. (23). Energy minimization proceeded until reaching the convergence criterion of $\Delta E < 1$ kcal/mol. The co-ordinate system for the global parameters was selected as follows: the long axial *X* co-ordinate axis for each TMH (1–7) was directed from the first to the last C^{α} atom; the *Y*-axis was perpendicular to *X* and went through the C^{α} atom of the 'middle' residue of each helix; and the *Z*-axis was built perpendicular to *X* and *Y* to maintain the right-handed co-ordinate system.

Docking of CPP ligands to the CXCR4 TMH bundle

The 11 CPPs (compounds **1**–**11**; Table 1) in the bioactive conformation suggested earlier (20) were docked to the 3D model of the CXCR4 TMH bundle. AutoDock 3.0 (28), assuming a rigid receptor with flexibility (rotation of bonds) of the ligand, was used for docking.

The t1 conformation of compound **1** (Table 2), which is a representation of the 3D pharmacophore model identified in our previous study (20), was selected as the reference conformation for ligand docking. The distal dihedral angles χ_3 of D-Tyr^2, χ_4 of Arg^4, and χ_2 of Nal^5 were not explicitly defined by the model, and were therefore allowed to rotate during docking, while the remaining torsion angles were fixed. The starting conformation for docking of compounds **2**–**11** was also taken from the low-energy conformations obtained by our systematic conformational search (20). The conformations were selected as the ones with lowest root-mean-

Table 1: Compounds included in the study, with affinities to CXCR4

Compound	Name	Sequence	IC_{50} (nM)[a]	Ref.
1	Ala^3FC131	c(Gly^1-D-Tyr^2-Ala^3-Arg^4-Nal^5)	63	(17)
2	D-NMe-Ala^3FC131	c(Gly^1-D-Tyr^2-D-NMe-Ala^3-Arg^4-Nal^5)	42	(17)
3	D-Ala^3FC131	c(Gly^1-D-Tyr^2-D-Ala^3-Arg^4-Nal^5)	230	(17)
4	Pro^3FC131	c(Gly^1-D-Tyr^2-Pro^3-Arg^4-Nal^5)	420	(17)
5	NMe-Ala^3FC131	c(Gly^1-D-Tyr^2-NMe-Ala^3-Arg^4-Nal^5)	490	(17)
6	*trans*-4-guanidino-Pro^3FC131	c(Gly^1-D-Tyr^2-*trans*-4-guanidino-Pro^3-Arg^4-Nal^5)	10	(17)
7	*cis*-4-guanidino-Pro^3FC131	c(Gly^1-D-Tyr^2-*cis*-4-guanidino-Pro^3-Arg^4-Nal^5)	10	(17)
8	FC131	c(Gly^1-D-Tyr^2-Arg^3-Arg^4-Nal^5)	4	(18)
9	D-Arg^3FC131	c(Gly^1-D-Tyr^2-D-Arg^3-Arg^4-Nal^5)	8	(18)
10	D-Arg^3-D-Nal^5FC131	c(Gly^1-D-Tyr^2-D-Arg^3-Arg^4-D-Nal^5)	16	(18)
11	Retro-inverso L-Tyr^2-D-Nal^5FC131	c(Gly^1-Nal^5-D-Arg^4-D-Arg^3-D-Tyr^2)	100–1000[b]	(19)

[a]Inhibition of stromal cell-derived factor-1α binding.
[b]IC_{50} value estimated from the EC_{50} value for anti-HIV activity (1.7 μM), as the anti-HIV activity of the cyclopentapeptides has been shown to correlate with affinity (18,19).

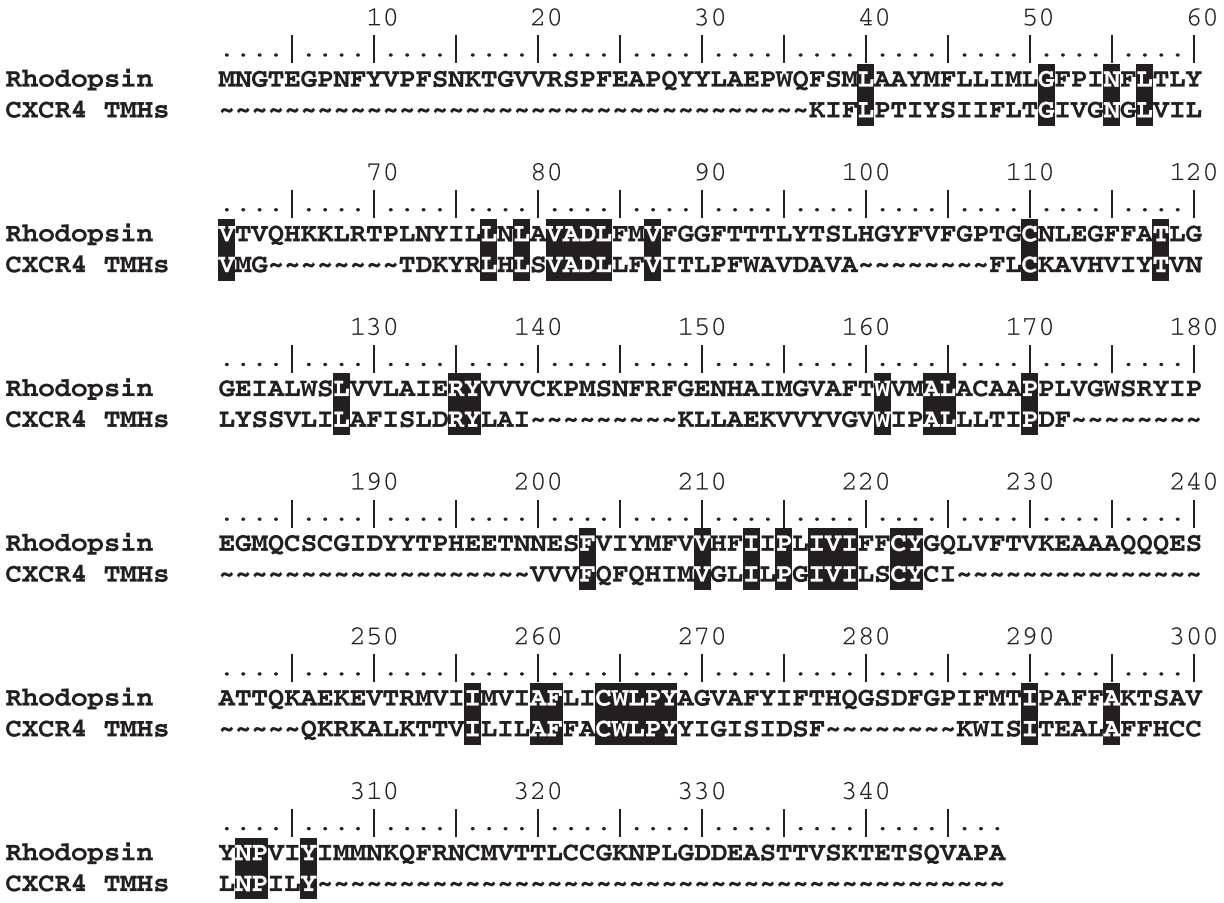

Figure 2: Final alignment of the transmembrane regions of CXCR4 with the rhodopsin sequence. Identical residues are shown with black background. Numbering is based on the rhodopsin sequence.

Table 2: Torsion angles (°) for conformation t1 of compound **1**, representing the three-point pharmacophore model (20)

Residue	φ	ψ	ω	χ_1	χ_2	χ_3	χ_4
Gly[1]	76	65	177	–	–	–	–
D-Tyr[2]	138	−103	180	177	105	180	–
Ala[3]	−68	−48	177	–	–	–	–
Arg[4]	−138	−59	−178	−175	174	178	140
Nal[5]	−107	81	−179	−62	117	–	–

squared deviation (RMSD) relative to conformation t1 of **1** based on the 10 atoms defining the 3D pharmacophore model (RMSD < 1 Å in all cases). These atoms were C^{ζ} of D-Tyr[2], C^{ζ} of Arg[4], $C^{\zeta 1}$ of Nal[5], O and H of the Xaa[3]-Arg[4] amide bond (representing the pharmacophoric points), and the five C^{α} atoms (representing the overall molecular volume); see also Figure 1. In the same way as for **1**, the three bonds defined by χ_3 of D-Tyr[2], χ_4 of Arg[4], and χ_2 of Nal[5] were allowed to rotate during docking of compounds **2**–**11**. For compounds **6**–**11**, the additional rotatable bonds in Xaa[3] were also allowed to rotate, giving a total of four rotated bonds for **6** and **7** and seven rotated bonds for **8**–**11**.

The initial preparation of receptor and ligands was carried out with SYBYL (Tripos, Inc., St Louis, MO, USA), and the graphical interface to AutoDock, AutoDockTools (ADT) (http://www.scripps.edu/mb/olson/doc/autodock/tools.html), was used to set up the actual docking. As the binding site for the CPPs was unknown, a grid map of 127^3 points with a spacing of 0.375 Å was used, which covered the whole TMH bundle with the exception of a few residues on the intracellular side. The Lamarckian genetic algorithm (LGA), which uses a combination of a genetic algorithm and a local search, was used as the search method. Each LGA docking was set to 100 runs with a random initial population of 100 individuals and the following parameters: maximum number of energy evaluations of 10^6 per rotated bond (3×10^6 for **1**–**5**, 4×10^6 for **6** and **7**, and 7×10^6 for **8**–**11**); maximum number of generations of 30 000 (making the search always terminate based on energy evaluations); quaternion and torsion steps of 5°; and translation step of 0.5 Å. The remaining docking parameters were set to the default values for the LGA search in ADT.

Comparison of poses

To identify the binding mode for the CPPs, the docked states (ligand conformation and orientation relative to the receptor; hereafter referred to as *poses*) of each compound were compared.

The LGA docking resulted in 100 poses for each of the 11 compounds. Intracompound clustering was performed within AutoDock using an RMSD threshold of 1.0 Å (all atoms, no translation). Only clusters found near or within the extracellular pocket formed by the seven TMHs as judged by visual inspection were considered further, i.e. clusters representing binding to the lipid-oriented face of the receptor were discarded.

For each of the remaining clusters, the pose with lowest docked energy was extracted as a representative. Based on the 10 atoms defining the 3D pharmacophore (see above), an in-house program was thereafter used for intercompound comparison between these poses, using an RMSD threshold of 3.0 Å (no translation). This resulted in the identification of two poses (termed A and B) that were common for all 11 compounds.

Optimization of ligand–receptor complexes

As the receptor structure is fixed in AutoDock, the interactions of poses A and B with the receptor were subsequently refined for the reference compound **1** using semiflexible receptor and ligand structures. The optimization (repacking) procedure was essentially the same as for packing of the seven TMHs (see above), with the exception that the ligand was introduced as the eighth component in the bundle, giving $6 \times 8 = 48$ 'global' parameters. The 'local' parameters were the dihedral angles of the side-chains for all helices, plus D-Tyr^2 χ_3, Arg^4 χ_4, and Nal^5 χ_2 of compound **1**.

Inspection of the two candidate ligand–receptor complexes for compound **1** revealed that the guanidino group of Arg^4 of **1** in both cases was in close proximity to the γ-carboxyl group of Glu288 in TMH7, but the geometry of the interaction was suboptimal. Therefore, the nine rotamers of the Glu288 side-chain were generated for both poses A and B, followed by reminimization of the complexes without further side-chain sampling. In both cases, this procedure resulted in complexes (termed 1A and 1B) with a more favorable interaction between Arg^4 and Glu288 and a lower overall energy than the initial complex sampled.

The A and B poses of compounds **2**–**11** were then optimized using the receptor structure of complexes 1A and 1B, respectively, to give a total of $2 \times 11 = 22$ ligand–receptor complexes (termed *X*A and *X*B; $X = 1$–11). This was performed by superimposing the pose onto **1** in the relevant complex using the 10 atoms of the 3D pharmacophore model (see above), followed by side-chain sampling and minimization as described for **1**. In the same way as for the docking, the dihedral angles χ_3 of D-Tyr^2, χ_4 of Arg^4, and χ_2 of Nal^5 were sampled for all compounds (**2**–**11**); for compounds **6**–**11**, the rotatable bonds in Xaa^3 were sampled additionally.

Results and Discussion

3D model of the CXCR4 TMH bundle

The final alignment of the transmembrane fragments of CXCR4 with the Rh sequence is shown in Figure 2. In addition to the overlap with the X.50 residues of Rh (24) for all TMHs, the alignment is in good agreement with the conservation pattern for the TMHs of 270 Rh-like GPCRs reported by Mirzadegan *et al.* (29).

The RMSD value (all C^α atoms) of the CXCR4 TMH bundle relative to the X-ray structure of Rh before and after helix packing was 1.56 and 2.35 Å, respectively.

Identification of candidate binding modes

The 11 CPPs (compounds **1**–**11**; Table 1) used as ligands for the docking studies were all high/medium affinity CXCR4 antagonists. Earlier, we have shown that they all display a small set of low-energy conformations compatible with the 3D pharmacophore model (20), indicating that all 11 compounds may share the same binding mode. Obviously, for compounds **6**–**11**, the additional guanidino group in Xaa^3 may contribute to a favorable receptor interaction not available to **1**–**5**. Our conformational study of these CPP CXCR4 antagonists revealed the bioactive conformation for all 11 compounds (20); see also Table 2.

For all compounds, the vast majority (>80%) of the docked poses found with AutoDock were located within the extracellular portion of the TMH bundle. The docking energy was not used as a criterion for selecting poses; however, the top-ranked poses were generally found within the TMH bundle (results not shown).

The relevant poses for each of the 11 ligands were then compared with each other (see Methods). We thereby identified two poses common to all ligands (poses A and B), representing candidate binding modes for the CPPs. Refinement of the ligand–receptor complexes based on these common poses using semiflexible receptor and ligand structures resulted in optimized interactions for the 22 complexes (*X*A and *X*B; $X = 1$–11).

Compatibility of the candidate binding modes with 3D pharmacophore model

Presumably, for the CPP–CXCR4 complex, the important pharmacophoric groups of the CPPs, as defined by our 3D pharmacophore model, should be involved in favorable interactions with their counterparts in CXCR4. The pharmacophore model predicts that such interactions may occur with the involvement of the D-Tyr^2 phenol group, the Arg^4 guanidino group, the Nal^5 naphthyl group, and the Xaa^3-Arg^4 amide bond. Additionally, the two amide bonds of the Gly^1-D-Tyr^2-Xaa^3 fragment, not explicitly considered in the model, but represented by the 'ideal' backbone conformation of compound **1**, could be involved in receptor interaction. The optimized complexes of the CXCR4 TMH bundle and the reference compound **1** (complexes 1A and 1B) are shown in Figure 3A,B, respectively, and the CXCR4 residues in proximity (<4 Å) of the pharmacophoric groups of **1** for each complex are listed in Table 3.

As is evident from Figure 3 and Table 3, there is a considerable degree of overlap between the two different binding modes in terms of the CXCR4 residues involved; however, the exact nature of the interactions differs. In complex 1A (Figure 3A), the OH group of D-Tyr^2 is H-bonded to the ε-amino group of Lys38 (TMH1), while the phenyl ring is in contact with Val99 (TMH2). The carbonyl group of the Ala^3-Arg^4 amide bond is H-bonded to the ε-amino group of Lys282 (TMH7), and is also within reach for H-bonding with the OH group of Ser285 (TMH7), even if the interaction (termed 'candidate H-bond') was not picked up in the optimization procedure. Moreover, the guanidino group of Arg^4 forms a salt bridge with Glu288 (TMH7), whereas the naphthyl ring of Nal^5 is surrounded by aromatic residues, i.e. His113 and Tyr116 (TMH3), and Tyr255 (TMH6). Thus, the binding mode represented by complex 1A is in good agreement with our pharmacophore model.

In complex 1B (Figure 3B) the OH group of D-Tyr^2 does not participate in any H-bonding as it protrudes out of the TMH bundle and into the extracellular space, while the phenyl ring is mainly in contact with Val196 (TMH5). A H-bond is observed between the NH group of the Gly^1-D-Tyr^2 amide bond and the side-chain carbonyl of Gln200 (TMH5), but not for the Ala^3-Arg^4 amide bond. However, the carbonyl oxygen of the Ala^3-Arg^4 amide bond is in close proximity to the basic residue His113 (TMH3), which may represent a positively charged local environment. Moreover, His113 represents a candidate H-bond partner, as rotation of its χ-angles would allow formation of a H-bond with the carbonyl group of the Ala^3-Arg^4 amide bond. In the same way as for complex 1A, Arg^4 and Glu288 (TMH7) form a salt bridge. In addition, the guanidino group of Arg^4 is in contact with the phenyl ring of Tyr116 (TMH3), which could represent a cation–π interaction, while the naphthyl ring of Nal^5 is mainly in contact with Tyr255 (TMH6) and Ile284 (TMH7).

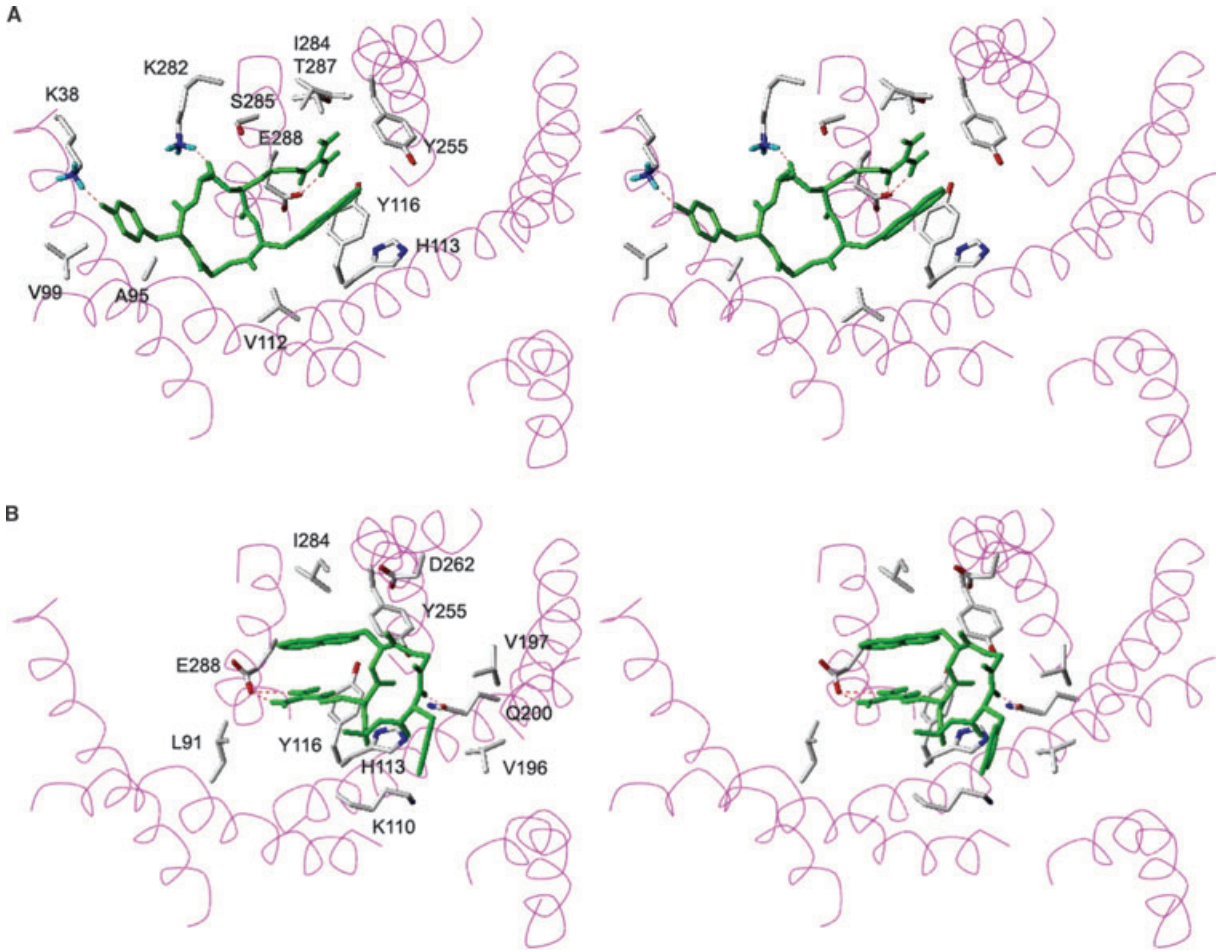

Figure 3: Stereoview of the optimized complexes of the reference compound 1 and the CXCR4 transmembrane helix (TMH) bundle (complexes 1A and 1B in A and B, respectively), representing the two candidate binding modes. Compound **1** is colored in green. The TMHs are represented by magenta ribbons, and only the side-chains of CXCR4 contact residues are displayed. H-bonds are shown as dotted red lines.

Accordingly, this binding mode is also in general agreement with the 3D pharmacophore.

For the A and B complexes of compounds **6**–**11**, the additional guanidino group in Xaa^3 was exposed to the extracellular environment, i.e. it was not involved in interactions with the TMH bundle (results not shown). Interestingly, the conformationally constrained guanidino group of compounds **6** and **7** was, in all cases, in proximity to Cys109 (TMH3), which is cysteine bridged to Cys186 in the extracellular loop (EL) 2. This orientation could potentially allow formation of a salt bridge between Xaa^3 and Asp187 in EL2.

Table 3: CXCR4 transmembrane helix residues in proximity (<4 Å) of the pharmacophoric groups of the reference ligand **1** after optimization of the two ligand–receptor complexes 1A and 1B

	CXCR4 contact residues	
Pharmacophoric groups	1A	1B
D-Tyr^2 side-chain	**Lys38**, Ala95, Val99	Val196, **Val197**, Gln200
Arg^4 side-chain	**Tyr116**, **Tyr255**, Ile284, Ser285, Thr287, **Glu288**	Leu91, **His113**, **Tyr116**, **Glu288**
Nal^5 side-chain	Val112, **His113**, **Tyr116**, **Glu288**	**Tyr255**, **Asp262**, Ile284
-NH-CO (Ala^3-Arg^4)	**Lys282**, Ser285	**Lys110**, **His113**, Gln200
-NH-CO (Gly^1-D-Tyr^2)	Ala95	Val196, **Val197**, Gln200
-NH-CO (D-Tyr^2-Ala^3)	Ala95, **Lys282**	**Lys110**, Val196, Gln200

Residues that have been subjected to relevant site-directed mutagenesis studies are shown in bold; see text for discussion and references.

In summary, based on the 3D models of the CPP–CXCR4 complexes, neither mode A nor mode B could be rejected as candidate binding modes. In favor of complex 1A is the fact that all important groups of the ligand, as described by the pharmacophore model, had counterparts in the receptor. The main argument against it is that the backbone groups of Arg^4 and Glu288 are in relatively close proximity (C^{α}–C^{α} distance of 7.1 Å), which should enable strong interactions also in the case of CPPs containing shorter Arg^4 analogs, e.g. guanidino-Dab. However, the guanidino-Dab^4 analog was shown to be a low-affinity compound (30). Also, the H-bond between the OH group of D-Tyr^2 and the ε-amino group of Lys38 (TMH1) was not seen for compounds **6**–**11**, probably as a result of electrostatic repulsion between the guanidino group of Xaa^3 and the ε-amino group of Lys38. Similarly, the H-bond between the carbonyl of the Xaa^3-Arg^4 amide bond and the ε-amino group of Lys282 (TMH7) was disrupted for compounds **9**–**11**. Besides, this binding mode involves interactions with residues in TMH1 and TMH2, which have been shown to be dispensable for the physiological function of CXCR4 (31).

In contrast, the binding mode of complex 1B mainly involves the CXCR4 'hot spot' comprised by TMH3, TMH5, TMH6, and TMH7. Here, the formation of the salt bridge between Arg^4 and Glu288 (TMH7) requires both residues to be in an extended conformation (C^{α}–C^{α} distance of 11.3 Å), which is in accordance with the affinity data for Arg^4-substituted CPP analogs (30). The main objection against this binding mode is that the Ala^3-Arg^4 amide bond is not explicitly involved in receptor interaction; however, as argued above, the orientation of this amide bond could still be important. Also, for the retro-inverso analog **11**, having reversed amide bonds, the H-bond between the side-chain carbonyl of Gln200 and the CPP backbone was shifted from Gly^1-D-Tyr^2 to Nal^5-Gly^1. The fact that the OH group of D-Tyr^2 did not interact with the TMH bundle does not mean that it does not have a counterpart in CXCR4 because its positioning could enable interaction with EL2.

Compatibility of the candidate binding modes with effects of point mutations in CXCR4 TMH bundle

No site-directed mutagenesis data are currently known for CXCR4 regarding binding of CPP antagonists. However, a number of such studies have been performed on CXCR4 to investigate the effects on the coreceptor activity for HIV entry (HIV gp120 envelope interactions), binding/signaling of the natural ligand SDF-1α, and binding of other CXCR4 antagonists. The N-terminus and the ELs of CXCR4 have been the focus of most of these studies, but a number of mutations in the TMH bundle have also been reported. As the CPPs have been shown to block binding of SDF-1α as well as HIV entry, the binding site of the CPPs is likely to overlap/interfere with the binding sites of both SDF-1α and HIV gp120. The literature data for point mutations of the CXCR4 TMH residues in contact with compound **1** (Table 3; Figure 3) relating to SDF-1α binding, HIV coreceptor activity or to other effects of relevance for the CPPs are summarized below for each of the two candidate binding modes.

For complex 1A, relevant mutation data were found for Lys38 (TMH1), His113 and Tyr116 (TMH3), Tyr255 (TMH6), and Lys282 and Glu288 (TMH7). The Lys38Ala mutation did not affect the anti-HIV activity of the CXCR4 antagonists T140 (32), which is a 14-residue peptide that formed the basis for the identification of FC131 (18,33,34). Similarly, the His113Ala mutation had no effect on the anti-HIV activity of T140 (32), and binding of Met-SDF-1α was also not significantly affected by this mutation (35). Neither Tyr116Ala nor Tyr255Ala was reported to affect the anti-HIV activity of T140 (32); however, the Tyr255Ala mutation was recently shown to reduce HIV coreceptor activity [<40% of wild type (WT)], without affecting SDF-1α binding and signaling to any extent (36). Lys282Ala was shown to have approximately the same coreceptor activity as WT by both Chabot *et al.* (37) and Brelot *et al.* (38). This mutation also did not affect the anti-HIV activity of T140 (32). Glu288 has received considerable attention, and has been mutated to Ala, Asp, and Gln. Rosenkilde *et al.* (39) reported dramatic impairment of SDF-1α signaling in the Glu288Ala mutant; however, the mutation was not shown to affect the anti-HIV activity of T140 (32). The Glu288Ala and Glu288Asp mutations were reported to reduce HIV coreceptor activity (<40% and 40–70% of WT, respectively), and both reduced SDF-1α signaling without any significant effect on binding (36). The Glu288Gln mutation has been shown to significantly reduce binding as well as signaling of SDF-1α (38).

For complex 1B, relevant data are available for Lys110, His113, and Tyr116 (TMH3), Val197 (TMH5), Tyr255 and Asp262 (TMH6), and Glu288 (TMH7). The effects of mutating His113, Tyr116, Tyr255, and Glu288 are discussed above. For Lys110Ala, a reduction in HIV coreceptor activity has been demonstrated by both Chabot *et al.* (37) and Brelot *et al.* (38); the mutation did not have any effect on the anti-HIV activity of T140 (32). In contrast, the Val197Asn mutant did not have any significant effect on HIV coreceptor function (40). In the same way as Glu288, Asp262 has been extensively studied, and mutated to Ala, Asn, and Asp. For the Asp262Ala mutant, both Chabot *et al.* and Brelot *et al.* have demonstrated reduced HIV coreceptor activity (37,38); more recently, a 10–30% reduction in HIV coreceptor activity was shown for this mutant, without any significant effect on SDF-1α binding and signaling (36). For the same mutant, however, Zhou and Tai (41) reported a significant reduction in SDF-1α binding. This mutation was also reported to affect the anti-HIV activity of T140, which was shown to be a result of reduced affinity of T140 for the mutant receptor (32). The Asp262Asn mutation did not influence binding of Met-SDF-1α to any extent (35), but it has been shown to affect HIV coreceptor activity (42,43). Similarly, Asp262Glu showed 30–60% reduction in HIV coreceptor activity, but did not affect SDF-1α binding and signaling to any extent (36).

As a consequence of different experimental approaches and the use of different HIV strains, the results from the site-directed mutagenesis studies are not totally consistent and somewhat difficult to interpret. However, Glu288 (TMH7) seems to be important for the HIV coreceptor activity of CXCR4 as well as for SDF-1α signaling, and possibly also for SDF-1α binding. Tyr255 and Asp262 (TMH6) also appear to be involved in interaction with HIV gp120, and there are some indications that Lys38 (TMH1) and Lys110 (TMH3) have some importance in this respect. Asp262 was identified as a contact residue for complex 1B, but does not seem to contribute favorably to ligand interaction. On the other hand, Glu288 and Tyr255

are involved in both of the two candidate binding modes for the CPPs, suggesting that the competing interaction of the CPPs with Glu288 and Tyr255 could be the reason for the inhibition of HIV entry by this class of compounds.

Comparison with other computational models of CXCR4–ligand interactions

Several attempts have been made to model ligand binding to CXCR4. A 3D model of CXCR4 in complex with SDF-1α has been proposed by Zhou *et al.* (44) using the experimentally determined X-ray structure of bacteriorhodopsin as template for the TMHs of CXCR4. The CXCR4–SDF-1α complex, generated by molecular dynamics (MD) simulation, only involved residues in the extracellular domain (N-terminus and ELs) of CXCR4. This is not in agreement with the commonly accepted two-site model for binding of SDF-1α that suggests an initial contact between SDF-1α and the N-terminus/ELs of CXCR4, followed by exposure of the CXCR4 TMH bundle to the N-terminus of SDF-1α (45). Consequently, the model by Zhou *et al.* does not provide information about TMH residues of importance for the function of CXCR4. It should also be mentioned that bacteriorhodopsin is not considered a suitable template for modeling of GPCRs because it is neither a GPCR itself nor does it show sequence homology with any GPCR.

Also based on MD simulations, Huang *et al.* (46) generated a model of the CXCR4–SDF-1α complex, in which dark-adapted rhodopsin was used as template for the TMH bundle. The results were in general accordance with the two-site model, as 'open' and 'closed' conformations of the extracellular CXCR4 domains were identified, where the 'open' conformation provided access to the CXCR4 TMH bundle. Dissociation of the salt bridge between Arg188 (EL2) and Glu277 (EL3) was proposed to be the key step for exposure of the transmembrane binding domain. This domain was composed of TMH3, TMH5, TMH6, and TMH7, and Asp262 (TMH6) was identified as the counterpart for Lys^1 of SDF-1α, which is critical for the agonist (signaling) function of SDF-1α (45). The other TMH residues involved in binding of SDF-1α were Tyr116, Gln200, Phe201, and Ile284. However, the identification of Asp262 as the important TMH residue for SDF-1α binding could be questioned because recent mutation data showed no effect of the Asp262Ala mutation on SDF-1α binding or signaling (36). With this exception, the results of the discussed computational study seem fairly consistent with both complexes 1A and 1B, but more so with 1B as the involvement of the same TMHs, and specifically Gln200 (TMH5), was predicted.

Similarly, Trent *et al.* (32) docked the antagonists T140 and AMD3100 to a rhodopsin-based CXCR4 model using MD simulation. The resulting complex of T140 involved the N-terminus, EL2 and EL3, and TMH4 and TMH5 of CXCR4, which was consistent with point mutation and cross-linking studies. The proposed binding mode for T140 involved a salt bridge between Arg^{14} of T140 (presumably corresponding to Arg^3 of FC131) and Asp171 (TMH4), which was not suggested for the CPPs in the present study. In our CXCR4 model, Asp171 forms the salt bridge with Lys110 (TMH3), and TMH4 is, to some extent, shielded from the main binding pocket by TMH3 and TMH5. Recent mutation data for Asp171 showed that this residue is of great importance for binding of HIV gp120 as well as SDF-1α (36). However, even if FC131 was 'derived' from T140, the residue contacts of the CPPs and the larger T140 do not necessarily have to be the same. This notion is supported by comparing the NMR structures of T140 (47) and FC131 (18), which reveals a different spatial arrangement of the C^{α} atoms of the pharmacophoric side-chains.

In contrast, the binding mode for AMD3100 suggested by Trent *et al.* (32) did not involve Asp171, but instead Asp262 and Glu288 as the primary interaction sites for the two positively charged cyclam rings, a finding which was supported by mutation data. The binding mode also involved two of the TMH residues identified as contacts for the CPPs in the present study, i.e. Tyr255 and Ile284. Thus, the suggested binding mode for AMD3100 shows considerable overlap with our two candidate modes for CPPs.

The finding by Trent *et al.* that Asp171 was not involved in binding to AMD3100 is in sharp contrast to the mutation data by Schwartz *et al.*, which has demonstrated the dependence of this residue for AMD3100 binding in several papers (35,39,48). Based on their experimental data, this group has suggested a simplistic 3D model for AMD3100 binding to CXCR4, which involves Asp171, Asp262, and Glu288 (39). One cyclam ring is proposed to interact with Asp171, while the other cyclam ring is 'sandwiched' between Asp262 and Glu288. This model is of limited value, however, as it was created simply by mutating residues in the dark-adapted Rh structure, followed by adjustment of side-chains and manual docking of AMD3100.

Rational design of CXCR4 mutants predicted to affect CPP binding

As discussed above, the available experimental data do not convincingly discriminate between the two candidate binding modes for CPPs suggested in the present study. A direct method to identify the most plausible mode would be to examine binding of CPPs to CXCR4 mutants designed to strengthen or weaken the specific residue–residue contacts listed in Table 3. As a result of the considerable degree of overlap between the two modes, i.e. contacts with His113 and Tyr116 (TMH3), Tyr255 (TMH6), and Ile284 and Glu288 (TMH7) in both cases, it would be reasonable to focus on mutants involving modifications of residues Lys38 in TMH1 (exclusive for complex 1A) and Gln200 in TMH5 (exclusive for complex 1B). Specifically, the following modifications can be envisioned: (i) alanine-scan mutants, such as Lys38Ala and Gln200Ala, where interactions between the ligand and the receptor in the binding modes A and B, respectively, would be weakened; (ii) mutations introducing steric conflicts in the binding site, e.g. substitution of Lys38 or Gln200 with Ile, Leu, or Trp to occupy spatial positions in the cavity between TMHs predicted for the binding modes A and B, respectively (see also Figure 3); and (iii) mutations introducing oppositely charged residues, such as Lys38Glu, aimed at interrupting the H-bonds and/or salt bridges between the receptor and the ligand. Obviously, to confirm that Glu288 is the key residue for interaction with the crucial Arg^4 of the CPPs, CPP binding studies with, for example, the Glu288Ala mutant is of immediate interest.

Conclusions

Based on the automated docking of CPP CXCR4 antagonist to a homology model of the CXCR4 TMH bundle, we have narrowed the 'binding space' for this compound class down to two plausible binding modes. Both of these are in general agreement with our independently generated 3D pharmacophore model for CPP binding to CXCR4, and both predict the involvement of Glu288 (TMH7) as the anchor point for this ligand class. The prediction is in line with existing data on site-directed mutagenesis of CXCR4 showing Glu288 as an important residue for HIV coreceptor activity and CXCR4–SDF-1α interaction. The present study provides a guide for the design of CXCR4 mutants to provide further experimental data on CPP binding to CXCR4, which in turn would facilitate the refinement of the CPP binding mode to CXCR4 and the search for CXCR4 antagonists with more drug-like properties.

Acknowledgments

J.V. acknowledges financial support from the Research Council of Norway (167113/V40). G.V.N. and G.R.M. acknowledge support from the National Institutes of Health (GM068460).

References

1. Bleul C.C., Farzan M., Choe H., Parolin C., Clark-Lewis I., Sodroski J., Springer T.A. (1996) The lymphocyte chemoattractant SDF-1 is a ligand for LESTR/fusin and blocks HIV-1 entry. Nature;382:829–833.
2. Oberlin E., Amara A., Bachelerie F., Bessia C., Virelizier J.-L., Arenzana-Seisdedos F., Schwartz O. et al. (1996) The CXC chemokine SDF-1 is the ligand for LESTR/fusin and prevents infection by T-cell-line-adapted HIV-1. Nature;382:833–835.
3. Feng Y., Broder C.C., Kennedy P.E., Berger E.A. (1996) HIV-1 entry cofactor: functional cDNA cloning of a seven-transmembrane, G protein-coupled receptor. Science;272:872–877.
4. Berson J.F., Long D., Doranz B.J., Rucker J., Jirik F.R., Doms R.W. (1996) A seven-transmembrane domain receptor involved in fusion and entry of T-cell-tropic human immunodeficiency virus type 1 strains. J Virol;70:6288–6295.
5. Tersmette M., de Goede R.E., Al B.J., Winkel I.N., Gruters R.A., Cuypers H.T., Huisman H.G. et al. (1988) Differential syncytium-inducing capacity of human immunodeficiency virus isolates: frequent detection of syncytium-inducing isolates in patients with acquired immunodeficiency syndrome (AIDS) and AIDS-related complex. J Virol;62:2026–2032.
6. Tersmette M., Lange J.M., de Goede R.E., de Wolf F., Eeftink-Schattenkerk J.K., Schellekens P.T., Coutinho R.A. et al. (1989) Association between biological properties of human immunodeficiency virus variants and risk for AIDS and AIDS mortality. Lancet;1:983–985.
7. Tersmette M., Gruters R.A., de Wolf F., de Goede R.E., Lange J.M., Schellekens P.T., Goudsmit J. et al. (1989) Evidence for a role of virulent human immunodeficiency virus (HIV) variants in the pathogenesis of acquired immunodeficiency syndrome: studies on sequential HIV isolates. J Virol;63:2118–2125.
8. Richman D.D., Bozzette S.A. (1994) The impact of the syncytium-inducing phenotype of human immunodeficiency virus on disease progression. J Infect Dis;169:968–974.
9. Connor R.I., Ho D.D. (1994) Human immunodeficiency virus type 1 variants with increased replicative capacity develop during the asymptomatic stage before disease progression. J Virol;68:4400–4408.
10. Connor R.I., Sheridan K.E., Ceradini D., Choe S., Landau N.R. (1997) Change in coreceptor use correlates with disease progression in HIV-1-infected individuals. J Exp Med;185:621–628.
11. Zhang L., He T., Huang Y., Chen Z., Guo Y., Wu S., Kunstman K.J. et al. (1998) Chemokine coreceptor usage by diverse primary isolates of human immunodeficiency virus type 1. J Virol;72:9307–9312.
12. De Clercq E. (2003) The bicyclam AMD3100 story. Nat Rev Drug Discov;2:581–587.
13. Ichiyama K., Yokoyama-Kumakura S., Tanaka Y., Tanaka R., Hirose K., Bannai K., Edamatsu T. et al. (2003) A duodenally absorbable CXC chemokine receptor 4 antagonist, KRH-1636, exhibits a potent and selective anti-HIV-1 activity. Proc Natl Acad Sci U S A;100:4185–4190.
14. Murakami T., Yoshida A., Tanaka R., Mitsuhashi S., Hirose K., Yanaka M., Yamamoto N. et al. (2004) KRH-2731: an orally bioavailable CXCR4 antagonist is a potent inhibitor of HIV-1 infection. In: 11th Conference on Retroviruses and Opportunistic Infections, February 8–11, 2004, San Francisco, CA, USA, Abstract No. 541.
15. Doranz B.J., Grovit-Ferbas K., Sharron M.P., Mao S.-H., Goetz M.B., Daar E.S., Doms R.W. et al. (1997) A small-molecule inhibitor directed against the chemokine receptor CXCR4 prevents its use as an HIV-1 coreceptor. J Exp Med;186:1395–1400.
16. Fujii N., Nakashima H., Tamamura H. (2003) The therapeutic potential of CXCR4 antagonists in the treatment of HIV. Exp Opin Invest Drugs;12:185–195.
17. Tamamura H., Araki T., Ueda S., Wang Z., Oishi S., Esaka A., Trent J.O. et al. (2005) Identification of novel low molecular weight CXCR4 antagonists by structural tuning of cyclic tetrapeptide scaffolds. J Med Chem;48:3280–3289.
18. Fujii N., Oishi S., Hiramatsu K., Araki T., Ueda S., Tamamura H., Otaka A. et al. (2003) Molecular-size reduction of a potent CXCR4-chemokine antagonist using orthogonal combination of conformation- and sequence-based libraries. Angew Chem Int Ed Engl;42:3251–3253.
19. Tamamura H., Mizumoto M., Hiramatsu K., Kusano S., Terakubo S., Yamamoto N., Trent J.O. et al. (2004) Topochemical exploration of potent compounds using retro-enantiomer libraries of cyclic pentapeptides. Org Biomol Chem;2:1255–1257.
20. Våbenø J., Nikiforovich G.V., Marshall G.R. (2006) A minimalistic 3D pharmacophore model for cyclopentapeptide CXCR4 antagonists. Biopolymers, in press; doi 10.1002/bip. 20508.
21. Palczewski K., Kumasaka T., Hori T., Behnke C.A., Motoshima H., Fox B.A., Le Trong I. et al. (2000) Crystal structure of rhodopsin: a G protein-coupled receptor. Science;289:739–745.
22. Nikiforovich G.V., Marshall G.R. (2001) 3D model for TM region of the AT-1 receptor in complex with angiotensin II independently validated by site-directed mutagenesis data. Biochem Biophys Res Commun;286:1204–1211.
23. Nikiforovich G.V., Mihalik B., Catt K.J., Marshall G.R. (2005) Molecular mechanisms of constitutive activity: mutations at position 111 of the angiotensin AT_1 receptor. J Pept Res;66:236–248.
24. Ballesteros J.A., Weinstein H. (1995) Integrated methods for the construction of three dimensional models and computational probing of structure–function relations in G-protein coupled receptors. Methods Neurosci;25:366–428.
25. Dunfield L.G., Burgess A.W., Scheraga H.A. (1978) Energy parameters in polypeptides. 8. Empirical potential energy algorithm for the conformational analysis of large molecules. J Phys Chem;82:2609–2616.
26. Nemethy G., Pottle M.S., Scheraga H.A. (1983) Energy parameters in polypeptides. 9. Updating of geometrical parameters, nonbonded interactions, and hydrogen bond interactions for the naturally occurring amino acids. J Phys Chem;87:1883–1887.
27. Nikiforovich G.V., Hruby V.J., Prakash O., Gehrig C.A. (1991) Topographical requirements for δ-selective opioid peptides. Biopolymers;31:941–955.
28. Morris G.M., Goodsell D.S., Halliday R.S., Huey R., Hart W.E., Belew R.K., Olson A.J. (1998) Automated docking using a Lamarckian genetic algorithm and an empirical binding free energy function. J Comput Chem;19:1639–1662.
29. Mirzadegan T., Benko G., Filipek S., Palczewski K. (2003) Sequence analyses of G-protein-coupled receptors: similarities to rhodopsin. Biochemistry;42:2759–2767.
30. Tamamura H., Esaka A., Ogawa T., Araki T., Ueda S., Wang Z., Trent J.O. et al. (2005) Structure–activity relationship studies on CXCR4 antagonists having cyclic pentapeptide scaffolds. Org Biomol Chem;3:4392–4394.
31. Ling K., Wang P., Zhao J., Wu Y.-L., Cheng Z.-J., Wu G.-X., Hu W. et al. (1999) Five-transmembrane domains appear sufficient for a G protein-coupled receptor: functional five-transmembrane domain chemokine receptors. Proc Natl Acad Sci U S A;96:7922–7927.

32. Trent J.O., Wang Z.-x., Murray J.L., Shao W., Tamamura H., Fujii N., Peiper S.C. (2003) Lipid bilayer simulations of CXCR4 with inverse agonists and weak partial agonists. J Biol Chem;278:47136–47144.
33. Tamamura H., Xu Y., Hattori T., Zhang X., Arakaki R., Kanbara K., Omagari A. et al. (1998) A low-molecular-weight inhibitor against the chemokine receptor CXCR4: a strong anti-HIV peptide T140. Biochem Biophys Res Commun;253:877–882.
34. Tamamura H., Omagari A., Oishi S., Kanamoto T., Yamamoto N., Peiper S.C., Nakashima H. et al. (2000) Pharmacophore identification of a specific CXCR4 inhibitor, T140, leads to development of effective anti-HIV agents with very high selectivity indexes. Bioorg Med Chem Lett;10:2633–2637.
35. Gerlach L.O., Skerlj R.T., Bridger G.J., Schwartz T.W. (2001) Molecular interactions of cyclam and bicyclam non-peptide antagonists with the CXCR4 chemokine receptor. J Biol Chem;276:14153–14160.
36. Tian S., Choi W.T., Liu D., Pesavento J., Wang Y., An J., Sodroski J.G. et al. (2005) Distinct functional sites for human immunodeficiency virus type 1 and stromal cell-derived factor 1α on CXCR4 transmembrane helical domains. J Virol;79:12667–12673.
37. Chabot D.J., Zhang P.-F., Quinnan G.V., Broder C.C. (1999) Mutagenesis of CXCR4 identifies important domains for human immunodeficiency virus type 1 X4 isolate envelope-mediated membrane fusion and virus entry and reveals cryptic coreceptor activity for R5 isolates. J Virol;73:6598–6609.
38. Brelot A., Heveker N., Montes M., Alizon M. (2000) Identification of residues of CXCR4 critical for human immunodeficiency virus coreceptor and chemokine receptor activities. J Biol Chem;275:23736–23744.
39. Rosenkilde M.M., Gerlach L.-O., Jakobsen J.S., Skerlj R.T., Bridger G.J., Schwartz T.W. (2004) Molecular mechanism of AMD3100 antagonism in the CXCR4 receptor: transfer of binding site to the CXCR3 receptor. J Biol Chem;279:3033–3041.
40. Wang Z.-x., Berson J.F., Zhang T.-y., Cen Y.-H., Sun Y., Sharron M., Lu Z.-h. et al. (1998) CXCR4 sequences involved in coreceptor determination of human immunodeficiency virus type-1 tropism. Unmasking of activity with M-tropic Env glycoproteins. J Biol Chem;273:15007–15015.
41. Zhou H., Tai H.-H. (2000) Expression and functional characterization of mutant human CXCR4 in insect cells: role of cysteinyl and negatively charged residues in ligand binding. Arch Biochem Biophys;373:211–217.
42. Hatse S., Princen K., Gerlach L.-O., Bridger G., Henson G., De Clercq E., Schwartz T.W. et al. (2001) Mutation of Asp171 and Asp262 of the chemokine receptor CXCR4 impairs its coreceptor function for human immunodeficiency virus-1 entry and abrogates the antagonistic activity of AMD3100. Mol Pharmacol;60:164–173.
43. Hatse S., Princen K., Vermeire K., Gerlach L.-O., Rosenkilde M.M., Schwartz T.W., Bridger G. et al. (2003) Mutations at the CXCR4 interaction sites for AMD3100 influence anti-CXCR4 antibody binding and HIV-1 entry. FEBS Lett;546:300–306.
44. Zhou N., Luo Z., Luo J., Liu D., Hall J.W., Pomerantz R.J., Huang Z. (2001) Structural and functional characterization of human CXCR4 as a chemokine receptor and HIV-1 co-receptor by mutagenesis and molecular modeling studies. J Biol Chem;276:42826–42833.
45. Crump M.P., Gong J.-H., Loetscher P., Rajarathnam K., Amara A., Arenzana-Seisdedos F., Virelizier J.-L. et al. (1997) Solution structure and basis for functional activity of stromal cell-derived factor-1; dissociation of CXCR4 activation from binding and inhibition of HIV-1. EMBO J;16:6996–7007.
46. Huang X., Shen J., Cui M., Shen L., Luo X., Ling K., Pei G. et al. (2003) Molecular dynamics simulations on SDF-1α: binding with CXCR4 receptor. Biophys J;84:171–184.
47. Tamamura H., Sugioka M., Odagaki Y., Omagari A., Kan Y., Oishi S., Nakashima H. et al. (2001) Conformational study of a highly specific CXCR4 inhibitor, T140, disclosing the close proximity of its intrinsic pharmacophores associated with strong anti-HIV activity. Bioorg Med Chem Lett;11:359–362.
48. Gerlach L.O., Jakobsen J.S., Jensen K.P., Rosenkilde M.R., Skerlj R.T., Ryde U., Bridger G.J. et al. (2003) Metal ion enhanced binding of AMD3100 to Asp^{262} in the CXCR4 receptor. Biochemistry;42:710–717.